Accepted Manuscript

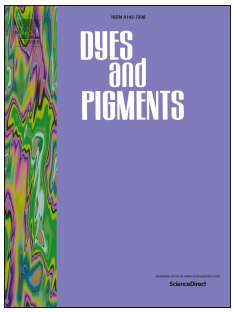

Schiff base derivatives containing thiodiazole: Twisted molecular conformation avoiding π … π stacking promotion aggregation-induced emission enhancement

Shun Yao, Xin Zhang, Haiyan Wang, Hui Wang, Xiaoping Gan, Zhichao Wu, Yupeng Tian, Zhongwen Pan, Hongping Zhou

PII: S0143-7208(17)30949-X

DOI: 10.1016/j.dyepig.2017.05.059

Reference: DYPI 6021

To appear in: *Dyes and Pigments*

Received Date: 25 April 2017

Revised Date: 28 May 2017

Accepted Date: 31 May 2017

Please cite this article as: Yao S, Zhang X, Wang H, Wang H, Gan X, Wu Z, Tian Y, Pan Z, Zhou H, Schiff base derivatives containing thiodiazole: Twisted molecular conformation avoiding π … π stacking promotion aggregation-induced emission enhancement, *Dyes and Pigments* (2017), doi: 10.1016/j.dyepig.2017.05.059.

The structure-property relationship of three new AIEE compounds were discussed, which showed the twisted molecular conformation avoiding π···π stacking facilitated aggregation-induced emission enhancement.

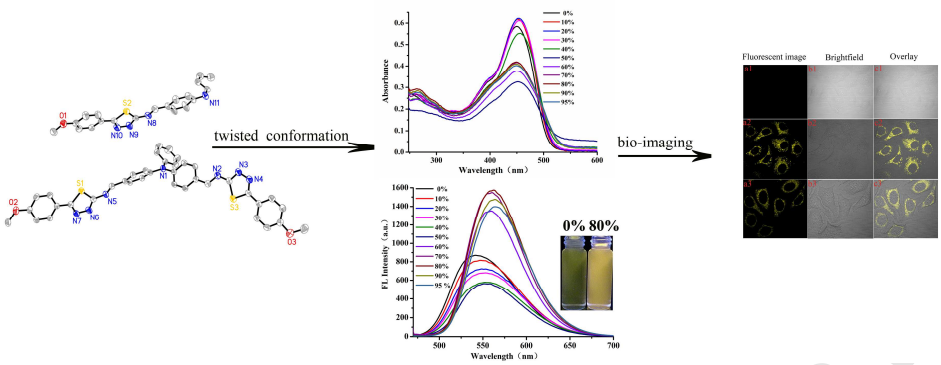

Schiff base derivatives containing thiodiazole: twisted molecular conformation avoiding π···π stacking promotion aggregation-induced emission enhancement

Shun Yao[a], Xin Zhang[a], Haiyan Wang[a], Hui Wang[a], Xiaoping Gan[b, c] *, Zhichao Wu[a], Yupeng Tian[a], Zhongwen Pan[a,] *, Hongping Zhou[a,] *

[a] *College of Chemistry and Chemical Engineering, Anhui University and Key Labotatory of Functional Inorganic Materials Chemistry of Anhui Province, Anhui Province Key Laboratory of Chemistry for Inorganic/Organic Hybrid Functionalized Materials, 230601, Hefei, P.R. China.*

[b] *School of Science, Anhui Agricultural University, 230036 Hefei, P. R. China.*

[c] *Co-operative Innovation Research Center for Weak Signal-Detecting Materials and Devices Integration, Anhui University, Hefei 230601, P. R. China.*

Corresponding author. Fax: +86-551-63861279

E-mail: zhpzhp@263.net

Abstract

Three novel 2-(4-methoxyphenyl)-1, 3, 4-thiadiazole based Schiff base derivatives (T1-T3) had been synthesized and characterized by ^{1}H NMR, ^{13}C NMR, MS and IR. The spectroscopic properties of T1-T3 were investigated by UV–*vis* absorption and fluorescence emission spectroscopy, which were coincident with theoretical calculations that three compounds possessed obvious intramolecular charge transfer (ICT) process. Their fluorescence emission performance in solution and aggregation state showed that three compounds all owned obvious aggregation-induced emission enhancement (AIEE) properties. To further understand AIEE nature, dynamic light scattering (DLS) and scanning electron microscopy (SEM) were comparatively investigated, which demonstrated that the small and uniform particles contributed to improve fluorescence emissions. Crystal structures of T1 and T3 showed that the twisted molecular conformation played an important role in AIEE. What's more, T2 and T3 had good biocompatibility, which were successfully applied in live-cell imaging.

Keywords: Schiff base, aggregation-induced emission enhancement, bio-imaging

1. Introduction

Designing novel chromophores with excellent optical properties in the condensed state had been a popular research area because of their potential applications in organic light-emitting diodes, light-emitting liquid crystals, circularly polarized luminescence (CPL), optical waveguides, and fluorescent sensors, especially fluorescent probe, which included chemical sensors, biological probes for cellular, bacterial and tissue imaging [1-4]. However, the frequently reported aggregation-caused quenching fluorescence (ACQ) occurred in common fluorescent molecules under high concentration solution or condensed state had greatly limited their potential applications. Fortunately, in 2001, Tang and co-workers firstly discovered a novel luminescence phenomenon defined as aggregation-induced emission (AIE), which could overcome the defect of ACQ [5-7]. In 2002, Park et al. also reported aggregation-induced emission enhancement (AIEE) materials were similar to AIE materials. The most popular AIE/AIEE mechanism at the single molecular level involved the restriction of intramolecular rotation (RIR) [8-10], *viz*, the σ bonds connecting the periphery phenyl rings and the core structure were able to rotate freely in dilute solution, which consumed the excited state energy and hence quenched the emission. However, in an aggregated state, such as nanoparticles or solid thin films/powders, the molecules were in a crowded neighborhood and these intramolecular motions were restricted, which diminished the non-radiative decay of the excited state energy and consequently induced strong emission [11]. According to the RIR mechanism, various excellent chromophores with aggregation-induced emission or enhanced emission (AIE/AIEE) properties had been developed, including tetraphenylethene (TPE), hexaphenylsilole (HPS), 1-methyl-pentaphenylsilole (MPPS), 1, 1-dimethyl-2, 3, 4, 5-tetraphenylsilole (DMTPS), distyreneanthracene (DSA), 2, 3-dicyano-5, 6-diphenylpyrazine, organoboron complexes and salicylaldehyde azine (SAA), and so on, which were widely applied in the novel luminogenic material [12-13]. These reported AIE/AIEE molecules effectively promoted the application of fluorescent probe in biological domain, while the new AIEE molecules still need further development，especially thiodiazole derivatives applied to luminescent material were rarely reported.

Thiodiazole derivatives had the vast potentials and demands in disinfection, weedicide, and sterilization due to it possessed a variety of biological activities [14]. Moreover,

thiodiazole molecule was also a highly conjugated aromatic heterocyclic which could be applied in optical materials. Triphenylamine had been widely used in opto- and electro-active materials due to its good electron-donating and hole-transporting capabilities, as well as the special propeller starburst molecular structure [15-16]. Schiff base compounds usually displayed superior AIEE property due to the isomerization/rotation of C=N group, and the intramolecular hydrogen bond which restricted the intermolecular rotation process[17-19].

Considering the factors mentioned above, a series of AIEE luminogenic compounds were developed by a simple preparation and purification at lower cost and shown in **Scheme 1**. The spectroscopic properties, DLS, SEM and crystal structure (T1 and T3) were researched in detail to elucidate the mechanism of enhanced fluorescence in the aggregated state, furthermore, T2 and T3 were successfully applied in live-cell imaging.

2. Experimental

2.1 Materials and instruments

Chemicals were purchased and used as received. Every solvent was purified as conventional methods beforehand. IR spectra were recorded with a Fourier transform infrared microscopy (VERTEX 80+HYPERION2000) in the 4000 - 400 cm^{-1} region. Melting points (uncorrected) were determined on a XT4 MP apparatus (Taike Corp., Beijing, China). ^{1}H and ^{13}C NMR were recorded on 400 MHz and 100 MHz NMR instruments using DMSO or $CDCl_3$ as solvent. Chemical shifts were reported in parts per million (ppm) relative to internal TMS (0 ppm) and coupling constants in Hz. Splitting patterns were described as singlet (s), doublet (d), triplet (t), quartet (q). The mass spectra were obtained on a Bruker Autoflex III smart beam mass spectrometer. The X-ray diffraction measurements were performed on a CCD area detector using graphite monochromated MoKa radiation (λ = 0.71069 (Å) at 298 (2) K. The non-hydrogen atoms were refined anisotropically and hydrogen atoms were introduced geometrically. Calculations were performed with SHELXTL-97 program package. Crystallographic data have been deposited with the Cambridge Crystallographic Data Centre as supplementary publication no. CCDC: 1498598 (for T1), 1498596 (for T3). DLS measurements were

conducted on a Malvern Zetasizer Nano ZS90 size analyzer. SEM images were obtained using a Zeiss MERLIN Compact. The one-photon absorption (OPA) spectra were recorded on the UV-3600 spectrophotometer and one-photon emission fluorescence (OPEF) spectra measurements were performed using a Hitachi F-7000 fluorescence spectrophotometer. The quartz cuvettes used were of 1 cm path length. The slit pass width of emission spectra: 10 nm, Voltage: 500 V.

2.2.1 Synthesis of 1

p-Anisic acid (3.04 g, 20 mmol) and thiosemicarbazide (1.82 g, 20 mmol) were dissolved in 30 mL of phosphorus oxychloride，the reaction mixture was refluxed at 85 ^{0}C for 10 h. After the reaction finished, the mixture was poured into ice water slowly and then saturate NaOH solution was added to adjust the pH value to 8.0 under vigorous stirring. The mixture was extracted with ethyl acetate three times and the organic layer was washed with brine and dried over anhydrous sodium sulfate. After solvent evaporation, the crude product was purified by recrystallization from anhydrous ethanol to get 3.15 g white powder, yield: 76.09%. Melting point: 188.1-189.5 ^{0}C. FT-IR (KBr, Disc, cm^{-1}): 3409.28 (m, ν_{NH2}), 3377.72 (m,ν_{NH2}), 3304.97 (w), 3105.35 (m), 1647.15 (m), 1608.48 (m, $\nu_{benzene}$), 1578.80 (w), 1511.49 (s, $\nu_{benzene}$), 1465.51(s), 1304.97 (w), 1267.34 (w), 1246.65 (s, ν_{OCH3}), 1174.54 (m, ν_{OCH3}), 1128.97 (w), 1052.67 (w), 1031.98 (m), 978.88 (w), 829.22 (m), 658.86 (w), 520.48 (w). ^{1}H NMR (DMSO-d_6, 400 MHz, ppm) δ: 7.69-7.67 (d, J = 8.0 Hz, 2H), 7.28 (s, 2H, NH_2), 7.03-7.01 (d, J = 8.0, 2H), 3.80 (s, 3H, OCH_3). ^{13}C NMR (100 MHz, DMSO) δ 167.85, 160.24， 156.25, 127.77, 123.61, 144.46，55.27. MS (ESI) m/z: found, $[M+H]^+$, 208.0542; molecular formula $C_9H_9N_3OS$ requires $[M+H]^+$, 208.0544.

2.2.2 Synthesis of 2-4

The compounds 2, 3 and 4 [20-21] were prepared according to the reported method.

2.2.3 Synthesis of T1-T3

Scheme 1 Preparation of compounds **T1**, **T2**, **T3**

T1 (0.271 g, 1 mmol) and compound 1 (0.248 g, 1.2 mmol) were dissolved in 15 mL of

anhydrous alcohol, the reaction mixture was refluxed at 70 ^{0}C for 12 h. After the reaction finished, the solution was cooled to room temperature, the solid was filtered and washed two times with anhydrous ethanol to give 0.37 g green solid, yield: 80.43 %. Melting point: 217.4-218.5 °C. FT- IR (KBr, Disc, cm^{-1}): 1601.19 (s, $\nu_{benzene}$), 1582.00 (m), 1558.11 (m), 1514.46 (s, $\nu_{benzene}$), 1445.05 (s), 1417.20 (m), 1360.58 (m), 1337.06 (m), 1312.98 (w), 1252.84 (m), 1224.75 (m, ν_{OCH3}), 1178.97 (m, ν_{OCH3}), 1159.28 (m, ν_{OCH3}), 825.46 (m), 737.66 (m), 718.23 (m). ^{1}H NMR (DMSO-d_6, 400 MHz, ppm) δ: 9.20 (s, 1H, CH=N), 8.38-8.36 (d, J = 8.0 Hz, 2H), 8.30-8.28 (d, J = 8.0 Hz, 2H), 7.98-7.91 (q, 4H), 7.58-7.56 (d, J = 8.0 Hz, 2H), 7.51-7.48 (t, 2H), 7.37-7.34 (t, 2H), 7.16-7.14 (d, J = 8.0 Hz, 2H), 3.85(s, 3H, OCH_3). ^{13}C NMR (100 MHz, $CDCl_3$) δ 172.83, 167.39, 165.10, 162.03, 142.39, 140.16, 133.11, 131.72, 129.25, 126.89, 126.27, 123.95, 123.25, 120.74, 120.49, 114.59, 109.86, 55.50.MS (ESI) m/z: found, $[M+H]^+$, 461.1427; molecular formula $C_{28}H_{20}N_4OS$ requires $[M+H]^+$, 461.1436.

T2 and T3 were obtained by following the similar procedure of T1.

T2: yellow powder, 0.35 g, yield: 75.76 %. Melting point: 184.6-185.7 ^{0}C. FT- IR (KBr, Disc, cm^{-1}): 1606.39 (m, $\nu_{C=N}$), 1582.88 (s), 1552.78 (m), 1509.19 (m, $\nu_{benzene}$), 1490.09 (m, $\nu_{benzene}$), 1442.73 (m), 1332.67 (m), 1301.00 (m), 1284.38 (m), 1257.11 (m), 1170.88 (s, ν_{OCH3}), 829.85 (w), 700.67 (w). ^{1}H NMR (DMSO-d_6, 400 MHz, ppm) δ: 8.83 (s, 1H, CH=N), 7.91-7.88 (q, 4H), 7.45-7.41 (t, J = 8.0, 4H), 7.26-7.21 (q, 6H), 7.12-7.10 (d, J = 8 Hz, 2H), 6.92-6.90 (d, J = 8Hz, 2H), 3.85 (s, 3H, OCH_3). ^{13}C NMR (100 MHz, DMSO) δ 173.37, 167.44, 164.88, 161.49, 152.32, 145.54, 131.83, 130.00, 128.86, 126.33, 125.44, 122.71, 118.58, 114.84, 55.47. MS (ESI) m/z: found, $[M+H]^+$, 463.1584; molecular formula $C_{28}H_{22}N_4OS$ requires $[M+H]^+$, 463.1592.

T3: orange solid, 0.48 g, yield: 70.69 %. Melting point: 239.3-240.6 ^{0}C. FT- IR (KBr, Disc, cm^{-1}): 1608.27 (m, $\nu_{benzene}$), 1587.27 (s), 1505.43 (s, $\nu_{benzene}$), 1444.61 (m), 1413.57 (w), 1325.46 (m), 1305.39 (m), 1287.21 (m), 1256.48 (s), 1168.06 (s, ν_{OCH3}), 832.15 (w). ^{1}H NMR (DMSO-d_6, 400 MHz, ppm) δ: 8.95(s, 2H, CH=N), 8.03-8.01 (d, J = 8.0, 4H), 7.94-7.91 (d, J = 12 Hz, 4H),7.52-7.49 (t, 2H), 7.36-7.32 (t, J = 8.0Hz, 1H), 7.28-7.20(q, 6H), 7.14-7.12 (d, J = 8.0 Hz, 4H), 3.86(s, 6H, OCH_3). ^{13}C NMR (100 MHz, $CDCl_3$) δ 173.37, 166.64, 165.22, 161.89, 151.20, 145.50, 131.70, 130.11, 129.32, 129.17, 126.96,

126.16, 123.38, 123.02, 114.52, 55.47. MS (ESI) m/z: found, $[M+H]^+$, 680.1889; molecular formula $C_{38}H_{29}N_7O_2S_2$ requires $[M+H]^+$, 680.1902.

3. Results and discussion

3.1 Spectroscopic properties

Fig. 1 Absorption (a) and fluorescence spectra (b) of **T2** in five organic solvents with different polarities at a concentration of 1×10^{-5} mol L^{-1}.

The absorption and fluorescence spectra were depicted in **Fig. 1** and **Fig. S2-S3**, the corresponding spectroscopic data were collected in **Table. S1**. Taking T2 as an example, it could be seen from **Fig. 1a** that T2 had two absorption peaks locted at ~293 nm and ~425 nm, respectively, the former was assigned to the π-π* electronic transition caused by the triphenylamine core whereas the latter was likely ascribed to intramolecular charge transfer between the triphenylamine core and the terminal group. **Fig. S2a-3a** showed T1 and T3 had similar feature in absorption spectra compared with T2. The fluorescence spectrum of T2 (**Fig. 1b**) exhibited one emission peak located from 528 nm to 568 nm in different polarity solvents, which was assigned to the ICT emission [22]. As shown in **Table. S1** and **Fig. 1b** the fluorescence emission of T2 was obvious red-shifted with increasing solvent polarity, **Fig. S2b-3b** presented T1 and T3 had the similar phenomenon compared with T2. Large stokes shifts were observed for the three compounds in five solvents due to strong solvent-solute dipole-dipole interactions, a manifestation of the large dipole moment and orientational polarizability. An increased dipole–dipole interaction between the solute and solvent generate a lower energy level. Stokes shift were approximately proportional to the orientational polarizability. To discuss the effect of solvents on the fluorescence spectrum, Lippert-Mataga plots for T1-T3 were given in **Fig. S4** and the calculation dates were collected in **Table S2 [**23-24].

$$\Delta\nu = \frac{2\Delta f}{4\pi\varepsilon_0\hbar c a^3}(\mu_e - \mu_g)^2 + b \qquad \text{Eq. (1)}$$

$$\Delta f = \frac{\varepsilon - 1}{2\varepsilon + 1} - \frac{n^2 - 1}{2n^2 + 1} \qquad \text{Eq. (2)}$$

in which $\Delta\nu = \nu_{abs} - \nu_{em}$ stands for Stokes shift, ν_{abs} and ν_{em} are absorption and emission

(cm^{-1}), h is the Planck constant, c is the velocity of light in vacuum, a is the Onsager radius and b is a constant. Δf is the orientation polarizability, μ_e and μ_g are the dipole moments of the emissive and ground states, respectively, and ε_0 is the permittivity of the vacuum. $(\mu_e - \mu_g)^2$ is proportional to the slope of the Lippert-Mataga plot. **Fig. S4** showed the slopes of the fitting line for compounds T1-T3 were as high as 17268, 10643 and 7066, respectively. The large slopes verified large dipole moment changes for these compounds, the large values of $\mu_e - \mu_g$ indicated that the molecule in the excited state had an extremely polar structure.

3.2 Electronic Structure

Fig. 2 Electron density distributions of the frontier molecular orbitals of compounds **T1-T3**

To understand the relationship between the optical properties and the electronic structure, the highest occupied and the lowest unoccupied molecular orbitals (HOMO and LUMO) were obtained by Gaussian 03 program and the B3LYP/6-31G basis sets based on crystal structure (T1 and T3) and optimized structure (T2), the results were similar to all of which based on optimized structure. Most of the electron clouds of the HOMO were evenly distributed in 9-phenyl-carbazole and triphenylamine part, while the majority of electron clouds of the LUMO were transferred and evenly distributed in the Schiff base (C=N) and 1, 3, 4-thiadiazole moieties, which revealed that absorption and emission of the three compounds originated from the ICT transitions [25]. It can be seen that the energy gaps calculated of the chromophores followed the order $\Delta E(T3) < \Delta E(T2) < \Delta E(T1)$ from **Fig. 2**, while the linear absorption wavelength increased in the order T3 > T2 > T1 in five solution, which were well consistent with experiments.

3.3 Aggregation-induced emission enhancement

Fig. 3 Absorption (a) and fluorescence spectra (b) of **T2** in ethanol/water mixtures with different f_w at a concentration of 1×10^{-5} mol L^{-1}. The inset depicts the changes of fluorescence intensity with different f_w.

Considering the three compounds were insoluble in water but soluble in organic solvents, we determined the absorption and emission spectra of the T1-T3 in organic/organic-water mixtures with different water fractions (f_w, the volume percentage of water in organic-water

mixtures, that can adjust the solvent polarity subtly), which were revealed by the images in **Fig. 3** and **Fig. S5-S6**. We used T2 as example to discuss the AIEE property. The absorption and fluorescence spectra of T2 were investigated in mixtures of ethanol/water with various water volume fractions (f_w). **Fig. 3a** showed T2 had a large absorption peaks at 430 nm, meanwhile, when $f_w \geq 70\%$, the absorption spectra started to show level-off tails in the long wavelength region caused by the Mie scattering effect, which indicated the formation of nanoaggregates. Similar effects of T1 and T3 were observed in **Fig. S5a-S6a**. The fluorescence spectra of T2 in the ethanol/water mixture with different water contents were shown in **Fig. 3b**, which exhibited a strong AIEE activity. When $f_w \leq 60\%$, the fluorescence (FL) intensity primarily decreased with increasing f_w, which was due to the increase of the solvent polarity and then transform to the twisted intramolecular charge transfer (TICT) state [26-27]. The light emission was invigorated from $f_w \geq 70\%$ and reached its maximum value at 90% water content, which was 4.2-fold higher than that in pure ethanol solution, accompanying a small red-shift in whole spectra. The increased in FL intensity can be attributed to the AIEE effect. We can also clearly see that the fluorescence spectra of T3 in ethanol/water mixtures had similar trend with that of T2 (**Fig. S6b)**. **Fig. S5b** showed that T1 had two emission peaks in dense THF solution, located at λ_{em1} (~450 nm) and λ_{em2} (~500 nm), which had a slightly difference compared with that of T2 and T3. As f_w increased, λ_{em1} disappeared gradually, the emission located at λ_{em2} increased correspondingly. The FL intensity was very weak accompanying with the slow increase as f_w from 0% to 60%, and a significant enhancement of fluorescence was observed when $f_w > 70\%$ accompanying a small red-shift in the spectrum. It was noteworthy that the fluorescence intensity of $f_w = 70\%$ lower than that of $f_w = 60\%$, this phenomenon was often observed in some compounds with AIEE properties [28-30], but the reasons remained unclear. There were two possible explanations for this phenomenon, first, after the aggregation, only the molecules on the surface of the nanoparticles emitted light and contributed to the fluorescence intensity upon excitation, leading to a decrease in fluorescence intensity. However, the restriction of intramolecular rotations of the aromatic rings in the aggregation state could enhanced light emission. The net outcome of these antagonistic processes depended on which process played a predominant role in affecting

the fluorescence behavior of the aggregated molecules. Second, when water was added, the solute molecules can aggregate into two kinds of nanoparticle suspensions: crystal particles and amorphous particles. The former leaded to an enhancement in the fluorescence intensity, while the latter leaded to a reduction in intensity. However, it was difficult to control the formation of nanoparticles in high water content. Thus, the measured fluorescence intensity often showed no regularity in high water.

Fig.4 Particle size distribution and SEM images of **T2** in the ethanol/water mixtures with different f_w at a concentration of 1×10^{-5} mol L^{-1}: (a, a1) in ethanol/water (20/80, v/v); (b, b1) in ethanol/water (10/90, v/v); (c, c1) in ethanol/water (5/95, v/v) .

To further elucidate the influence of morphology and particle size on AIEE properties, SEM and DLS studies were supplemented. As shown in **Fig. 4**, the size distribution of T2 were 241.2 nm (f_w = 80%), 135.3 nm (f_w = 90%) and 164.0 nm (f_w = 95%) respectively, which was conducted by DLS in solvent mixtures with high water ratios. SEM was used to observe the aggregation, which were also well certified the nano-level aggregation of T2 at the same water fractions as DLS. The results illustrated that the enhanced emission was related to the small and uniform particles, the reason may be that the weak intermolecular interactions could work efficiently under ordered aggregation condition. **Fig. S7**-**S8** showed that T1 and T3 had the similar size distribution influence on AIEE properties in mixture solution.

3.4 Mechanisms of emission enhancement

Crystal structure was most important for us to understand the optoelectronic properties and molecular packing, which will help deeply our understanding of luminescence processes and guided us to develop new AIEE systems. Single crystals of T1 and T3 were obtained by slow evaporation from the solutions in dichloromethane / acetonitrile at room temperature. The crystal structures of T1 and T3 were shown in **Fig. 5** and **Fig. S9**. Their crystallographic dates were summarized in **Table. S3**. The ORTEP diagrams of T1 and T3 with the N, O and S atom numbering schemes and some of the packing interactions in the crystals were depicted in **Fig. 5a** and **Fig. S9a**.

As shown in **Fig. 5b** and **Fig. S9b**, the dihedral angles between the plane of the 1, 3,

4-thiadiazole ring and the adjacent benzene ring are 5.85° for T1 and 7.98° for T3, which indicated that the T1 and T3 had good planarity. For compound T1, we could see that the C-H···N hydrogen bonds (*d* = 2.494 Å ∠C18-H18···N3 = 173.66°) and C-H··π weak interactions (C8-H8··π, *d* = 2.894 Å) played significant role in the growth of 1D chain, then the 2D layer structure formed through C-H···N hydrogen bonds (*d* = 2.724 Å ∠C5-H5··N4 = 134.89°) (**Fig. 5c-5d**). However, the vertical distances between the terminal benzene ring and double bonds (C=N) was 3.454 Å and the slip angles was 33.90° in the neighboring molecules, which indicated the molecule had π··π packing interactions (**Fig. 5e**), this was why T1 only possessed weak FL intensity in aggregation state.

For compound T3, every two molecules were packed into a small unit, the adjacent three small units were stacked together to form the 1D chain structure *via* three kinds of C-H··O hydrogen bonds (*d* = 2.521 Å, ∠C50-H50-O1 = 147.22°, *d* = 2.501 Å, ∠C5-H5-O2 = 145.04° and *d* = 2.664 Å ∠C1-H1-O3 = 151.02°) and two kinds of C-H··π interactions (C54-H54··π, *d* = 2.813 Å and C24-H24··π, *d* = 2.842 Å) (**Fig. S9c)**. Furthermore, the two 1D chain structure were connected to form the 2D layer structure through C-H··π (C33-H33··π, *d* = 2.820 Å) interactions (**Fig. S9d)**. The results illustrated that twisted molecular conformation could avoid π···π stacking and boost aggregation induced emission enhancement.

Fig. 5 Crystal structure of **T1**, (a) ORTEP diagram of **T1**, (b) The dihedral angles of **T1**, (c) The 1D linear structure of **T1**, (d) The 2D linear structure of **T1**,(e)The π··π stacking.

3.5 Cell Imaging

To explore the application in biology for T1-T3, the bio-imaging experiments were carried out by confocal laser scanning microscopy using HepG2 cells as an example. The tested compounds were dissolved in DMSO and then serially diluted in complete culture medium. The excitation wavelength was fixed at their maximum absorption wavelength in microscopy imaging. From **Fig.6 a2-a3**, we can see that the bright-yellow fluorescence mainly focused on the cytoplasm for T2 and T3, which confirmed that the two compounds both had good biocompatibility and could enter into the cells and aggregate in the cytoplasm successfully. But, any fluorescence in live-cell for T1 could not observed

although we had tried many times (**Fig. 6a1)**, which could be attributed the weak FL intensity caused by the particular molecular structure

Fig. 6 (a1 - a3) Fluorescence image of HepG2 cells with **T1-T3** after 15min of incubation and washed with PBS buffer. (b1 - b3) Bright-field images, (c1 - c3) Merged images

4. Conclusion

In summary, three AIEE-active compounds have been designed and synthesized by subtle structure adjustment. Their fluorescence emission performance in ethanol/water or THF/water solutions were obviously different, DLS and SEM images of the compounds revealed that the small and uniform particles were in favor of fluorescence emissions. Crystal structure demonstrated that the structural variations had a great influence on photophysical properties, molecular packing, electronic structure, and aggregation-induced fluorescence properties. Furthermore, T2 and T3 were successfully applied to label the cytoplasm in live cells, which could offer a new direction for developing biological probe based on AIEE luminophores.

Acknowledgements

This work was supported by General Program of National Natural Science Foundation of China (51472002, 51432001), Science and Technology Plan of Anhui Province (1604b0602016), the Ministry of Education of China, Higher Education Revitalization Plan Talent Project of Anhui Province (2013) and Open Foundation of Co-operative Innovation Research Center for Weak Signal-Detecting Materials and Device Integration of Anhui University (Y01008411).

Reference

[1] Odabas S, Tekin E, Turksoy F, Tanyeli C. Synthesis of new N-heteroaromatic attached tetraphenylethene based luminogens having aggregation induced emission and their applications in organic light emitting diodes. Journal of Luminescence 2016;176:240-9.

[2] Han TY, Hong YN, Xie N, Chen SJ, et al. Defect-sensitive crystals based on diaminomaleonitrile-functionalized Schiff base with aggregation-enhanced emission. Journal of Materials Chemistry C 2013;1(44):7314-20.

[3] Zhou J, Chang ZF, Jiang YB, He BR, Du M, Lu P, Zhao ZJ, et al. From tetraphenylethene to tetranaphthylethene: structural evolution in AIE luminogen continues. Chemical Communications 2013;49(25):2491-3.

[4] Viglianti L, Leung NLC, Xie N, Gu XG, Sung HH, Miao Q, Williams ID, Licandro E, Tang BZ. Aggregation-Induced Emission: Mechanistic Study of Clusteroluminescence of Tetrathienylethene. Chemical Science 2017;8:2629-39.

[5] Yoshii R, Nagai A, Tanaka K, Chujo Y. Highly Emissive Boron Ketoiminate Derivatives as a New Class of Aggregation□Induced Emission Fluorophores. Chemistry–A European Journal 2013;19(14):4506-12.

[6] Zhao ZJ, Deng CM, Chen SM, Lam JW, Qin W, Lu P, Wang ZH, Kwok HS, Ma YG, Qiu HY, Tang BZ. Full emission color tuning in luminogens constructed from tetraphenylethene, benzo-2, 1, 3-thiadiazole and thiophene building blocks. Chemical Communications 2011;47(31):8847-9.

[7] Jiang YH, Wang YC, Hua JL, Tang J, Li B, Qian SH, Tian H. Multibranched triarylamine end-capped triazines with aggregation-induced emission and large two-photon absorption cross-sections. Chemical Communications 2010;46(26):4689-91.

[8] Wang D, Li SM, Zheng JQ, Kong DY, Zheng XJ, Fang DC, Jin LP. Coordination-Directed Stacking and Aggregation-Induced Emission Enhancement of the Zn (II) Schiff Base Complex. Inorganic Chemistry 2017;56(2):984-90.

[9] Kwok RTK, Geng JL, Lam JWY, Zhao EG, Wang G, Zhan RY, Liu B, Tang BZ. Water-soluble bioprobes with aggregation-induced emission characteristics for light-up sensing of heparin. Journal of Materials Chemistry B 2014;2(26):4134-41.

[10] Wang LK, Zheng Z, Yu ZP, Zheng J, Fang M, Wu JY, et al. Schiff base particles with aggregation-induced enhanced emission: random aggregation preventing π–π stacking. J Mater Chem C 2013;1(42):6952-9.

[11] Hu RR, Kang Y, Tang BZ. Recent advances in AIE polymers. Polymer Journal 2016;48:359-70.

[12] Feng Q, Li YY, Wang LL, Li C, Wang JM, Liu YY, Li K, Hou HW. Multiple-color aggregation-induced emission (AIE) molecules as chemodosimeters for pH sensing. Chemical Communications 2016;52(15):3123-26.

[13] Wang LK, Shen YF, Yang MD, Zhang XZ, Xu WN, Zhu QJ,Wu JY, Tian YP, Zhou HP. Novel highly emissive H-aggregates with aggregate fluorescence change in a phenylbenzoxazole-based system. Chemical Communications 2014;50(63):8723-6.

[14] Shang XF, Li WL, Wei XF, Zhang HL, Fu ZY, Zhang JL, Xu XF. Synthesis, Bioactivity, and the Anion□Binding Property of 2□Sulfydryl□1, 3, 4□thiodiazole Derivatives. Heteroatom Chemistry 2015;26(2):142-9.

[15] Ning Z, Tian H. Triarylamine: a promising core unit for efficient photovoltaic materials.Chem. Commun 2009;37:5483-95.

[16] Liu YQ, Kong M, Zhang Q., Zhang ZW, Zhou HP, Zhang SY, Li SL, Wu JY, Tian YP. A series of triphenylamine-based two-photon absorbing materials with AIE property for biological imaging. Journal of Materials Chemistry B 2014;2(33):5430-40.

[17] Zhang X, Huang XD, Gan XP, Wu ZC, Yu JH, Zhou HP, Tian YP. Two multi-Functional aggregation-Induced emission probes: Reversible mechanochromism and bio-imaging. Sensors and Actuators B: Chemical 2017;243:421-8.

[18] Gan XP, Liu GJ, Chu MJ, et al. Intermolecular interactions boost aggregation induced emission in carbazole Schiff base derivatives. Organic Biomolecular Chemistry 2017;15(9): 2119-2119.

[19] Lou XD, Zhao ZJ, Hong YN, et al. A new turn-on chemosensor for bio-thiols based on the nanoaggregates of a tetraphenylethene-coumarin fluorophore. Nanoscale 2014;6(24): 14691-96.

[20] Shao HX, Chen XP, Wang ZX, Lu P. Synthesis and fluorescence properties of carbazole and fluorene-based compounds. Journal of Luminescence 2007;127(2):349-54.

[21] Thomas M, Said G, Meziane M, Mireille B. Olivier M. Practical and efficient synthesis of tris (4-formylphenyl) amine, a key building block in materials chemistry. Synthesis 2005;11:1771-4.

[22] Ji S, Yang J, Yang Q, Liu SS, Chen MD, Zhao JZ. Tuning the intramolecular charge transfer of alkynylpyrenes: effect on photophysical properties and its application in design of OFF− ON fluorescent thiol probes. The Journal of organic chemistry 2009;74(13):4855-65.

[23] Grabowski ZR, Rotkiewicz K, Rettig W. Structural changes accompanying intramolecular electron transfer: focus on twisted intramolecular charge-transfer states and structures. Chem. Rev 2003;103(10),3899-4032.

[24] Patel SA, Cozzuol M, Hales JM, Richards CI, Sartin M, et al. Electron transfer-induced blinking in Ag nanodot fluorescence. The Journal of Physical Chemistry C 2009;113(47):20264-70.

[25] Gan XP, Wang Y, Ge XP, Li W, Zhang X, Zhu W, et al. Triphenylamine isophorone derivatives with two photon absorption: Photo-physical property, DFT study and bio-imaging. Dyes Pigments 2015;120:65-73.

[26] Hu RR, Lager E, Aguilar-Aguilar A, Liu JZ, et al. Twisted intramolecular charge transfer and aggregation-induced emission of BODIPY derivatives. The Journal of Physical Chemistry C 2009;113(36):15845-53.

[27] Qin W, Ding D, Liu JZ, Yuan WZ, Hu Y, Liu B, Tang BZ. Biocompatible Nanoparticles with Aggregation□Induced Emission Characteristics as Far□Red/Near□Infrared Fluorescent Bioprobes for In Vitro and In Vivo Imaging Applications. Advanced Functional Materials 2012;22(4):771-9.

[28] Zhang XQ, Chi ZG, Xu BJ, Li HY, Yang ZY, et al. Synthesis of blue light emitting bis (triphenylethylene) derivatives: a case of aggregation-induced emission enhancement. Dyes and Pigments 2011;89(1):56-62.

[29] Zhang XQ, Chi ZG, Xu BJ, Chen CJ, Zhou X, Zhang Y,Liu SW, Xu JR. End-group effects of piezofluorochromic aggregation-induced enhanced emission compounds containing distyrylanthracene. Journal of Materials Chemistry 2012;22(35):18505-13.

[30] Xu BJ, Chi ZG, Li HY, Zhang XQ, Li XF, et al. Synthesis and properties of aggregation-induced emission compounds containing triphenylethene and

tetraphenylethene moieties. The Journal of Physical Chemistry C 2011;115(35):17574-81.

Figure captions

Scheme 1 Preparation of compounds **T1**, **T2**, **T3**.

Fig. 1 Absorption (a) and fluorescence spectra (b) of **T2** in five organic solvents with different polarities at a concentration of 1×10^{-5} mol L^{-1}.

Fig. 2 Electron density distributions of the frontier molecular orbitals of compounds **T1**-**T3**.

Fig. 3 Absorption (a) and fluorescence spectra (b) of **T2** in ethanol/water mixtures with different f_w at a concentration of 1×10^{-5} mol L^{-1}. The inset depicts the changes of fluorescence intensity with different f_w .

Fig.4 Particle size distribution and SEM images of **T2** in the ethanol/water mixtures with different f_w at a concentration of 1×10^{-5} mol L^{-1}: (a, a1) in ethanol/water (20/80, v/v); (b, b1) in ethanol/water (10/90, v/v); (c, c1) in ethanol/water (5/95, v/v).

Fig. 5 Crystal structure of **T1**, (a) ORTEP diagram of **T1**, (b) The dihedral angles of **T1**, (c) The 1D linear structure of **T1**, (d) The 2D linear structure of **T1**,(e)The weak $\pi\cdots\pi$ stacking.

Fig. 6 (a1 - a3) Fluorescence image of HepG2 cells with **T1**-**T3** after 15min of incubation and washed with PBS buffer. (b1 - b3) Bright-field images, (c1 - c3) Merged images.

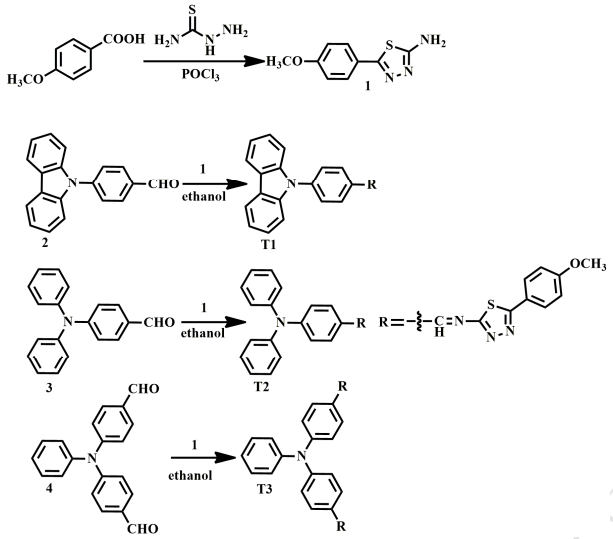

Scheme 1 Preparation of compounds **T1**, **T2**, **T3**

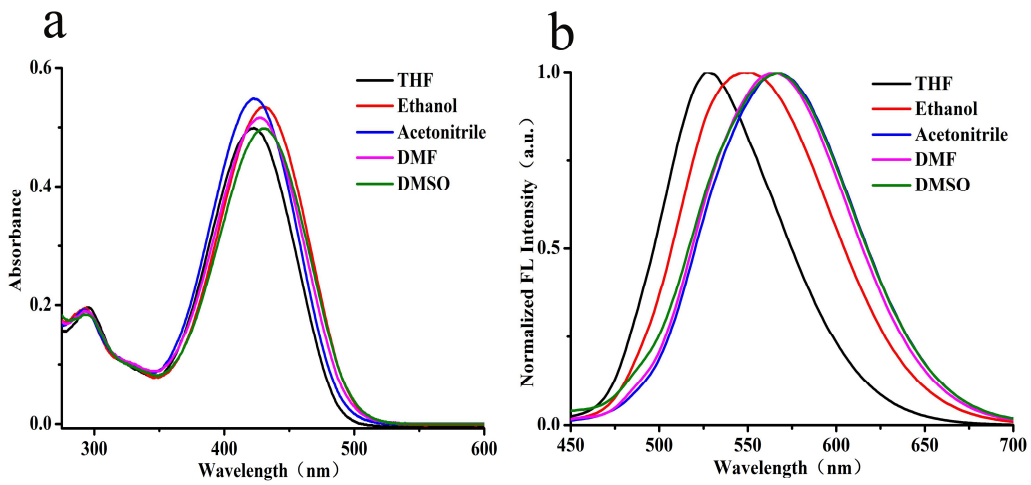

Fig. 1 Absorption (a) and fluorescence spectra (b) of **T2** in five organic solvents with different polarities at a concentration of 1×10^{-5} mol L^{-1}.

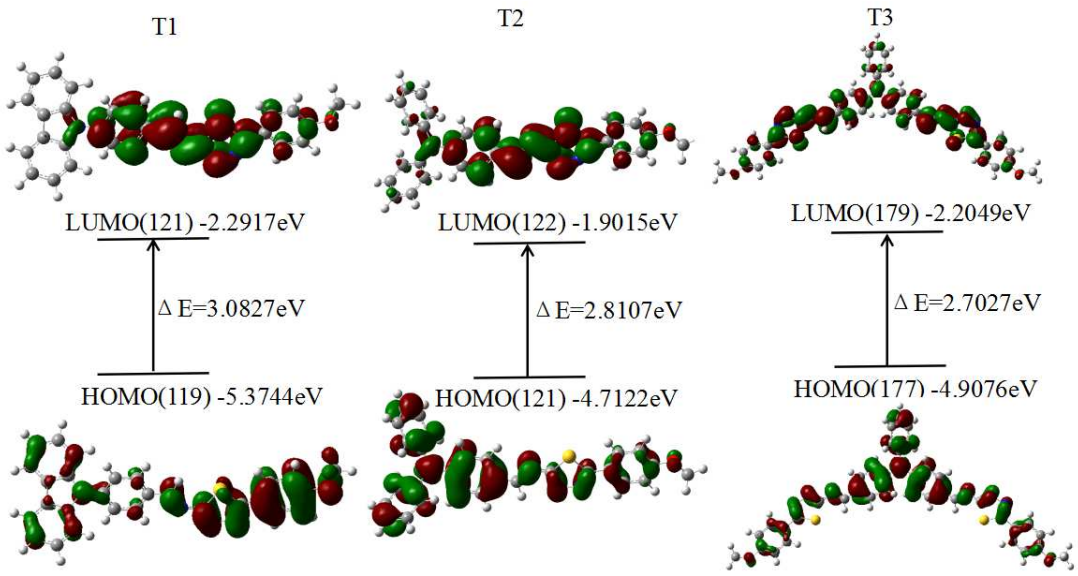

Fig. 2 Electron density distributions of the frontier molecular orbitals of compounds **T1-T3**

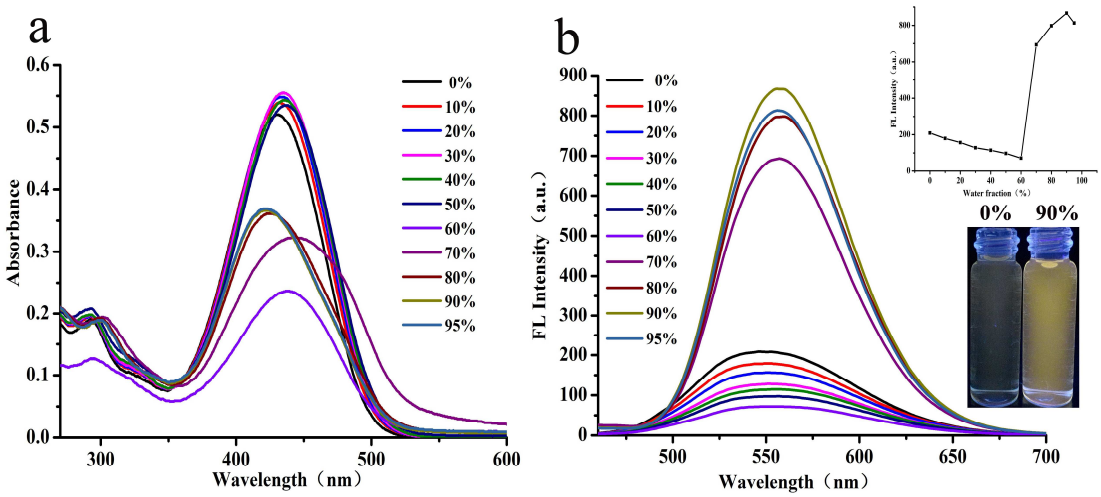

Fig. 3 Absorption (a) and fluorescence spectra (b) of **T2** in ethanol/water mixtures with different f_w at a concentration of 1×10^{-5} mol L^{-1}. The inset depicts the changes of fluorescence intensity with different f_w .

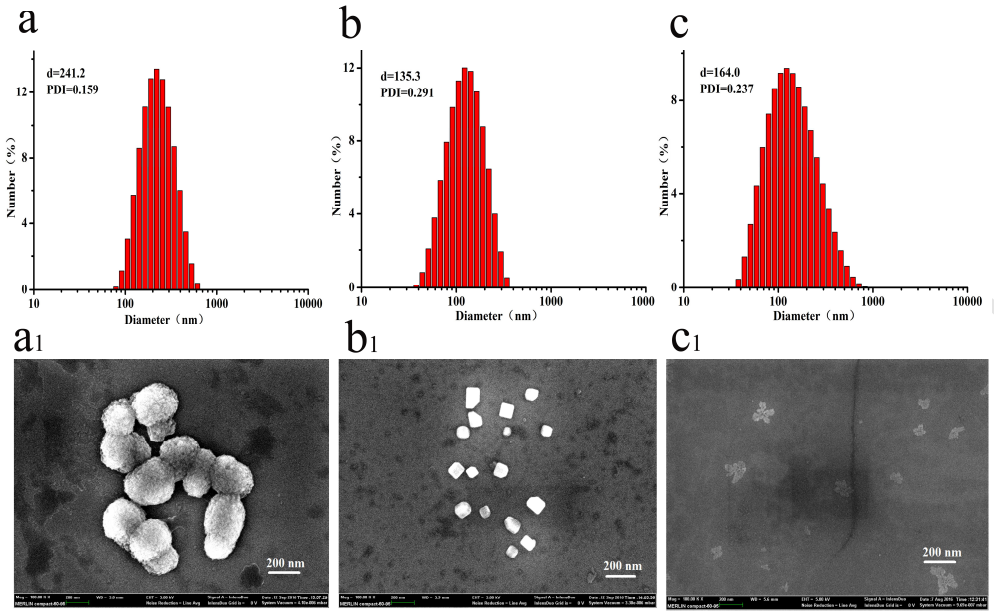

Fig.4 Particle size distribution and SEM images of **T2** in the ethanol/water mixtures with different f_w at a concentration of 1×10^{-5} mol L^{-1}: (a, a1) in ethanol/water (20/80, v/v); (b, b1) in ethanol/water (10/90, v/v); (c, c1) in ethanol/water (5/95, v/v) .

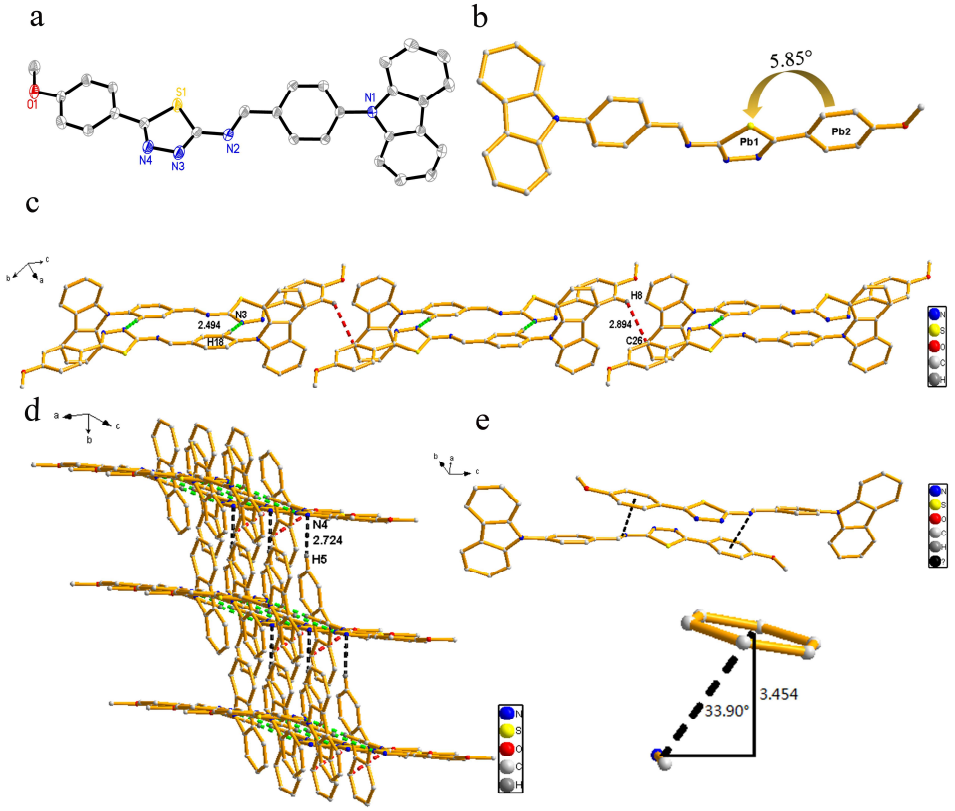

Fig. 5 Crystal structure of **T1**, (a) ORTEP diagram of **T1**, (b) The dihedral angles of **T1**, (c) The 1D linear structure of **T1**, (d) The 2D linear structure of **T1**,(e)The weak π···π stacking.

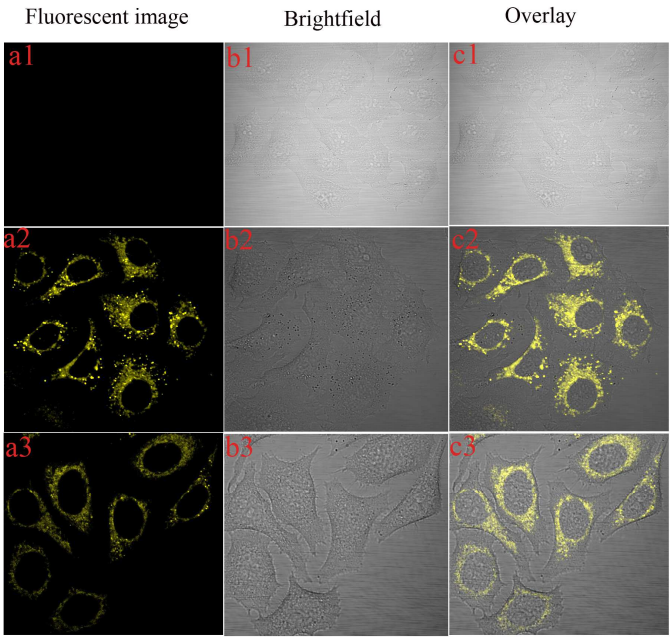

Fig. 6 (a1 - a3) Fluorescence image of HepG2 cells with **T1-T3** after 15min of incubation and washed with PBS buffer. (b1 - b3) Bright-field images, (c1 - c3) Merged images

Highlights

- The structures of T1 and T3 were determined by single crystal X-ray diffraction analysis.
- The twisted molecular conformation facilitated aggregation-induced emission enhancement.
- T2 and T3 were applied in live cell imaging, which highlighted their practical performance.